Soil Carbon Losses Reduce Soil Moisture in Global Climate Model Simulations

SONALI SHUKLA MCDERMID,[a,c] ENSHENG WENG,[b,c] MICHAEL PUMA,[b,c] BENJAMIN COOK,[c,d] TOMISLAV HENGL,[e] JONATHAN SANDERMAN,[f] GABRIELLE J. M. DE LANNOY,[g] AND IGOR ALEINOV[b,c]

[a] *Department of Environmental Studies, New York University, New York, New York*
[b] *Center for Climate Systems Research, Columbia University, New York, New York*
[c] *NASA Goddard Institute for Space Studies, New York, New York*
[d] *Lamont-Doherty Earth Observatory, Columbia University, Palisades, New York*
[e] *OpenGeoHub Foundation/Enviromatrix Ltd., Wageningen, Netherlands*
[f] *Woodwell Climate Research Center, Woods Hole, Massachusetts*
[g] *Department of Earth and Environmental Sciences, Katholieke Universiteit Leuven, Leuven, Belgium*

(Manuscript received 24 January 2022, in final form 5 July 2022)

ABSTRACT: Most agricultural soils have experienced substantial soil organic carbon losses in time. These losses motivate recent calls to restore organic carbon in agricultural lands to improve biogeochemical cycling and for climate change mitigation. Declines in organic carbon also reduce soil infiltration and water holding capacity, which may have important effects on regional hydrology and climate. To explore the regional hydroclimate impacts of soil organic carbon changes, we conduct new global climate model experiments with NASA Goddard Institute for Space Studies ModelE that include spatially explicit soil organic carbon concentrations associated with different human land management scenarios. Compared to a "no land use" case, a year 2010 soil degradation scenario, in which organic carbon content (OCC; weight %) is reduced by a factor of ~0.12 on average across agricultural soils, resulted in soil moisture losses between 0.5 and 1 temporal standard deviations over eastern Asia, northern Europe, and the eastern United States. In a more extreme idealized scenario where OCC is reduced uniformly by 0.66 across agricultural soils, soil moisture losses exceed one standard deviation in both hemispheres. Within the model, these soil moisture declines occur primarily due to reductions in porosity (and to a lesser extent infiltration) that overall soil water holding capacity. These results demonstrate that changes in soil organic carbon can have meaningful, large-scale effects on regional hydroclimate and should be considered in climate model evaluations and developments. Further, this also suggests that soil restoration efforts targeting the carbon cycle are likely to have additional benefits for improving drought resilience.

KEYWORDS: Atmosphere-land interaction; Anthropogenic effects/forcing; Biosphere-atmosphere interaction; Climatology; Soil moisture; Water budget/balance

1. Introduction

Land-use and land-cover change, especially through agricultural expansion and industrialization, has resulted in soil organic matter losses across many important crop and pasture regions (Sanderman et al. 2017; Scholes et al. 2018). Hereafter, we refer primarily to soil organic matter in terms of stored soil organic carbon (SOC), as this constitutes a major portion (~58%) of total organic matter in soils. The global SOC stock to 1 m depth amounts to ~1500 PgC, although significant spatial variation exists (Zomer et al. 2017). The weight fraction of organic carbon content (OCC) of most agricultural soils is <2% of the total mass of soil material and concentrated in the upper soil layers (Oldfield et al. 2019). Consequently, small OCC changes are associated with relatively large declines in stocks of SOC, and these changes have significant impacts on soil ecosystem services (Lal et al. 2011). Since the dawn of agriculture (~12 000 years), global SOC stocks have declined by an estimated ~116 PgC as a consequence of land-use change (Sanderman et al. 2017). These losses have had significant impacts on nutrient retention and cycling in agricultural systems, with implications for reduced productivity (Lal et al. 2011; Oldfield et al. 2019), while also contributing to rising atmospheric greenhouse gas concentrations (Lal 2015; Lal et al. 2015; Houghton and Nassikas 2017). In light of this, there is growing interest in rebuilding soil carbon stocks on agricultural land through improved management to mitigate anthropogenic climate change (Chabbi et al. 2017; Amelung et al. 2020; Bossio et al. 2020; Zomer et al. 2017; Paustian et al. 2016).

Additionally, there are also important *biogeophysical* impacts of SOC changes, particularly related to soil–water dynamics in managed agroecosystems (Arenas-Calle et al. 2021). Higher SOC content increases porosity and stabilizes soil aggregates, thereby increasing soil water holding capacity and plant available water (Intergovernmental Technical Panel on Soils 2015). As an example, in a major Canadian agricultural region with relatively high SOC, Manns et al. (2016) identified strong correlative relationships and feedbacks between SOC,

Ensheng Weng, Michael Puma, Benjamin Cook, and Tomislav Hengl made equal contributions.

Corresponding author: Sonali Shukla McDermid, sps246@nyu.edu

Earth Interactions is published jointly by the American Meteorological Society, the American Geophysical Union, and the Association of American Geographers.

DOI: 10.1175/EI-D-22-0003.1

© 2022 American Meteorological Society. For information regarding reuse of this content and general copyright information, consult the AMS Copyright Policy (www.ametsoc.org/PUBSReuseLicenses).

Unauthenticated | Downloaded 03/28/23 09:33 AM UTC

soil textures, and mean soil water content (positively correlated with SOC). In fact, Herrick et al. (2013) suggest that significant losses of SOC, and corresponding degradation of soil structures, may lead to "edaphic droughts" that persist during mean or "normal" growing (i.e., precipitation) conditions. Losses of SOC could potentially exacerbate climate-driven variability and drought.

As a possible corollary, increasing SOC may help to partially ameliorate drought impacts on crops, thereby serving as an adaptive strategy for agricultural systems under climate change (Arenas-Calle et al. 2021; Webb et al. 2017; Iizumi and Wagai 2019; Williams et al. 2016). Conservation soil management, which can protect and restore SOC through cover cropping, perennial plantings, and other practices, has been shown to increase infiltration relative to standard management practices by ~30%–60% (Basche and DeLonge 2019; Blanco-Canqui et al. 2015). Across major maize growing regions in the United States, higher soil organic matter is associated with reduced rates of crop insurance payouts during droughts, related at least in part to higher available water capacity (Kane et al. 2021) as well as other plant and soil interactions that have yet to be understood and quantified. A global empirical analysis by Iizumi and Wagai (2019) demonstrated that enhancing SOC can benefit crop productivity during dry years, thereby partially mitigating crop risks due to drought and/or in rainfed agroclimatic zones (Lal et al. 2007). For coarse textured soils in Wisconsin, Yost and Hartemink (2019) found that a 1% increase in SOC was correlated with 0.05 m^3 m^{-3} additional plant available water. The mean plant available water across soils in this study was only 0.11 m^3 m^{-3} suggesting that an increase of organic carbon from 1 to 3 weight % would improve plant available water by around 50% on a relative basis.

Nevertheless, the debate continues regarding if and to what degree a given increase in SOC increases plant available water (Minasny and McBratney 2018; Krull et al. 2004). Sources of uncertainty include limitations in large regional or global databases and heterogeneity of soils; pedotransfer functions that may not capture the full variability in soil water (Minasny and McBratney 2018); and/or the variation in cultivated soils (e.g., Loveland and Webb 2003) and experimental design and treatments (e.g., Blanco-Canqui et al. 2015; Lal et al. 2007). We further note that increased soil water under conservation management is likely related not just to increases in SOC, but also to increased root growth, soil faunal activity associated with a denser rooting system, and resulting soil aggregates that collectively decrease bulk density, increase porosity, and can lead to enhanced infiltration. It is therefore important to consider and account for the ways agricultural management impacts the diversity of organic and biological matter in soils when considering their impact on water infiltration (Cardoso et al. 2013). In general, SOC-mediated increases in plant available water may become more consequential near field capacity than near the soil wilting point (Minasny and McBratney 2018; Hudson 1994) and for coarse-textured (e.g., sandy) soils (Rawls et al. 2003). Hudson (1994), nevertheless, found that plant available water more than doubled as soil organic matter content increased from 0.5% to 3% across texture classes. However, as Minasny and McBratney (2018) note, increasing soil organic matter levels by 2% or more throughout the rooting zone (top half meter) of many agricultural soils may be an overly ambitious management goal.

Global and regional experiments have been conducted with land surface and climate models (with varying degrees of process coupling) to investigate the carbon cycle and biogeochemical consequences of soil carbon changes (Drewniak et al. 2015; Tian et al. 2016; Luo et al. 2016; Ito et al. 2020). However, few studies have explored the biogeophysical effects of soil carbon, especially on soil moisture and hydroclimate (Rawls et al. 2003). De Lannoy et al. (2014) did explicitly account for the effects of soil OCC for relatively low-carbon soils in calculations of soil hydraulic parameters (e.g., porosity, saturated hydraulic conductivity, and matric potential) in global land surface model experiments. While this constitutes an important avenue of model development, additional work is needed to assess the contribution of these developments to regional hydroclimate in a coupled modeling framework. In this study, we begin to fill this research gap by linking soil organic carbon changes to biogeophysical (i.e., hydroclimate) responses in the NASA Goddard Institute for Space Studies ModelE (Kelley et al. 2020) global climate model. Specifically, we conduct a sensitivity study to investigate how scenarios of SOC change, driven largely by anthropogenic land-use and land-cover change, impact key soil hydraulic parameters and modify global and regional soil moisture and hydroclimate.

2. Methods

a. *Description of the NASA GISS ModelE*

We perform our experiments with the NASA GISS ModelE, a state-of-the-art global climate model that contributes to the Coupled Model Intercomparison Project (CMIP) (Eyring et al. 2016) as an ongoing development effort. The most recent documented version, with spatial resolution is 2° latitude × 2.5° longitude and 40 vertical atmospheric layers, is described in Kelley et al. (2020), Miller (2014), and Schmidt et al. (2014). ModelE has been shown to reasonably represent observed climate conditions and responses to historical anthropogenic forcings (Miller 2014; Schmidt et al. 2014). For this study, we use prescribed sea surface temperatures reflecting climatological conditions around the year 2000 and superimposed the detrended historical sea surface temperature variability from 1850 to 1985, resulting in 136 years of simulation time. All other forcings, anthropogenic and natural including greenhouse gases, aerosols, volcanoes, etc., were set to year 2000 conditions (Table 1), as was global land use (crop and pasture fractions) (McDermid et al. 2019). The last 130 years of the integration are used for our analyses.

ModelE uses vegetation characteristics from the Ent Terrestrial Biosphere Model (Ent TBM) (Kim et al. 2015). For our experiments, we operate Ent in "biophysics-only" mode as described by Kim et al. (2015). Ent biophysics are based on well-known coupled photosynthesis and stomatal conductance formulation (Ball et al. 1987; Collatz et al. 1991; Farquhar and von Caemmerer 1982). Further details about the natural vegetation phenology and

Unauthenticated | Downloaded 03/28/23 09:33 AM UTC

TABLE 1. Short names and descriptions of ModelE experiments conducted for this study.

Expt short name	Description
NoLU	SOC layers down to 100 cm adapted from no-land-use scenario in Sanderman et al. (2017)
2010LU	SOC layers down to 100 cm adapted from 2010 land-use scenario in Sanderman et al. (2017)
30ST	A sensitivity test constructed by reducing NoLU SOC by 30%; this value represented the approximate 95th percentile of losses under 2010 land-use conditions (relative to NoLU)

the canopy radiative transfer can be found in Kim et al. (2015) and Friend and Kiang (2005), respectively. In this mode, water vapor fluxes are prognostically simulated for each grid cell by prescribing canopy structure and leaf area index (LAI) for 17 possible plant functional types. Rooting depth across the plant functional types are currently given by Rosenzweig and Abramopoulos (1997). More than 60% of the root mass for crop functional type gridcell fractions are located within the top ~0.6 m of soil in this vegetation structure. All soil moisture results that follow are average values over this depth. Over agricultural grid cells, LAI values and seasonal cycles (i.e., crop calendars) for crop-designated plant functional types are prescribed in accordance with McDermid et al. (2019).

The land module with ModelE (see appendix for more information) includes two tiles within each terrestrial grid cell: one with bare soil and the other with vegetated soil. For each tile, the six-layer soil column extends to a depth of 3.5 m, where the layer thicknesses are computed using a geometric progression of 0.1, 0.17, 0.30, 0.51, 0.89, and 1.53 m (Rosenzweig and Abramopoulos 1997). Soil composition in the model is characterized as a mixture of five different components: sand, silt, and clay, the distributions of which were obtained from SoilGrids (Hengl et al. 2017) (see section 2b below). Peat and bedrock layers were unchanged from default ModelE configuration (Staub et al. 1987; Webb et al. 1991, 1993). TerraE includes a representation of infiltration and redistribution (Abramopoulos et al. 1988) using Richards' equation in one dimension with sink terms for evaporation and transpiration (e.g., Abramopoulos et al. 1988; Puma et al. 2007). The constitutive equations for the relationships between soil moisture and both matrix potential and hydraulic conductivity are based on the empirical Campbell (1974) formulations. Details on these formulations as well as runoff, evaporation, and transpiration are provided in the appendix.

For this study, we update TerraE with new soil saturated hydraulic parameters (SHPs) for the Campbell (1974) equations (see appendix). The new SHPs were calculated offline using the pedotransfer functions (PTFs) detailed in De Lannoy et al. (2014) (see their Tables 1 and 2, also in appendix), which were adapted from Saxton and Rawls (2006) and Wösten et al. (2001, 1999). We choose these PTFs because they account for the influence of lower levels of soil carbon (i.e., lower than those found in peatlands or organic soils, which are higher than carbon levels that characterize many agricultural regions) on the SHPs.

b. *Soil organic carbon data and model implementation*

Global, spatially explicit data on SOC stocks (MgC ha^{-1}) were obtained from Sanderman et al. (2017) and soil bulk densities and textures (sand, silt, clay, and coarse fractions) were provided by SoilGrids (Hengl et al. 2017) at a 5 arc min spatial resolution. SOC stocks were provided for anthropogenic land-use (LU) conditions reflecting reference years 900, 1800, 1910, 1960, 1990, and 2010 CE ("2010LU"), as well as a no-land-use ("NoLU") scenario, taken to be ~10 000 BC based on the previous work of Sanderman et al. (2017). These scenarios contain the SOC concentrations for 0–30, 0–100, and 0–200 cm soil depth, but do not provide data on the associated bulk density or texture. Therefore, we will rely on the available soil bulk density values and textures from SoilGrids, which correspond to 2010 conditions, and this will limit our ability to capture important SOC feedbacks with bulk density. We consider the limitations this may impose on our findings in the discussion section (section 4) below. From the available LU scenarios above, we selected the 2010LU, representing near-modern day conditions, for comparison to the NoLU scenario (Table 1). The 2010LU scenario is characterized by a spatially variable reduction of the SOC across agricultural land (OCC reduced by a factor 0.12) relative to the NoLU.

For these two selected scenarios, the SOC data were implemented in ModelE per the steps shown in Fig. 1 as follows:

1) The SHP calculations require soil carbon to be expressed as weight percentage OCC. Therefore, SOC (mass, kg) stock data given by the Sanderman et al. scenarios were converted to OCC (weight %) for the "top" (0–30 cm)

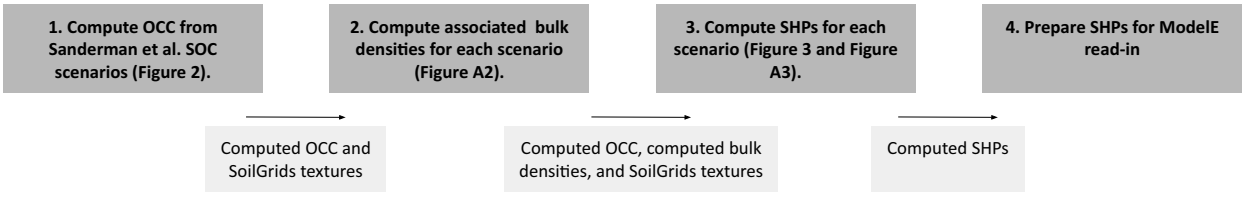


FIG. 1. Flow diagram of approach for implementing SOC scenarios in the GISS ModelE land surface. Dark gray boxes indicate the calculation steps performed (described in section 2b) and light gray boxes specify the available inputs to each calculation.

Unauthenticated | Downloaded 03/28/23 09:33 AM UTC

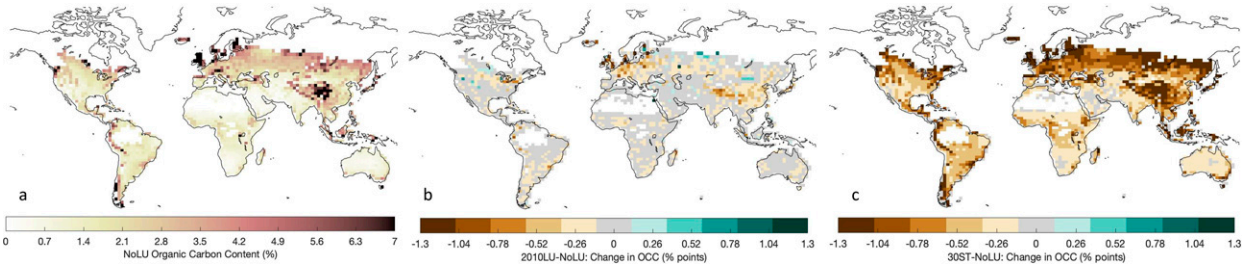


FIG. 2. (a) OCC (weight %) for NoLU conditions down to 100 cm. Change in OCC (change expressed in percentage points) from NoLU for the (b) 2010LU and (c) 30ST experiments. All maps are masked for modern (~2000s) combined crop and pasture area in order to focus on the responses of human-managed land systems.

and "profile" (0–100 cm) soil layers using the bulk density and textures provided by SoilGrids (which represent present-day soil conditions).

2) These fractional OCC values are then taken as "given" and, together with SoilGrids' mineral soil texture weight fractions, are used to compute new, spatially explicit bulk densities for each scenario with PTFs provided in De Lannoy et al. (2014) (Fig. A1b). These computed bulk density values are then used for all subsequent SHP calculations. As a point of comparison, we note that the 2010LU OCC values produced in step 1 result in computed bulk densities (here in step 2) that are generally lower than those shown in De Lannoy et al. (2014) (see Fig. A2), particularly across mid–high latitudes. We discuss implications of this below.
3) Using the computed OCC values from step 1, the computed bulk densities from step 2, and the SoilGrids textures, we compute the SHPs for the "top" and "profile" soil layers using the PTFs detailed in De Lannoy et al. (2014) (see their Table 2 and Fig. A1). We also calculate the associated wilting point using Campbell (1974), and all calculations are performed at the native 5 arc min SoilGrids resolution. For these calculations, OCC is converted to organic matter content using 1.72 scaling factor.
4) We aggregate these SHPs to the coarser ModelE resolution using a nearest neighbor approach and apply the spatially explicit values uniformly over the six ModelE soil layers as they correspond to either the respective "top" or "profile" thicknesses. These aggregated SHP layers are then read in as an input file for ModelE simulations.

c. *Experimental design*

In addition to the NoLU and 2010LU scenarios, we also construct a sensitivity test reducing NoLU SOC uniformly by 30% (OCC reduced by 0.66 weight %) (Table 1) across all agricultural grid cells and at depth. This value represented the spatial 95th percentile of losses for the 2010LU scenario relative to NoLU. We note it has also been estimated that many key agricultural regions have lost ~30% (or more) of SOC to date (Lal et al. 2015), and so this value may reflect a plausible upper limit.

Figures 2 and 3 show how OCC and SHPs differ for the various scenarios. The 2010LU scenario shows key areas of OCC loss, including across East Asia/China, western Europe, and the northern U.S. Midwest, relative to NoLU (Fig. 2a). This results in collocated declines in porosity, a measure of potential maximum soil water holding capacity, exceeding 5% across these areas (Fig. 3a). Saturated hydraulic conductivity also displays declines, particularly across these midlatitude growing regions (Fig. 3c), and increases in matric potential (Fig. A3), which may in theory contribute to plant water stress. Per our experimental design of the 30ST scenario, OCC losses (Fig. 2c) and their effect on conductivity and soil water holding capacity (Figs. 3b,d) are much more widespread and severe.

We note, however, that our land surface and vegetation model is run with prescribed leaf area indexes for all plant functional types, and thus we do not expect vegetation in these simulations to display large sensitivities to the possible soil water changes shown here. We therefore hypothesize that our implementation of soil carbon changes will primarily impact soil water holding capacity and possibly infiltration (and therefore runoff to an extent). Future work will include explicitly coupled, dynamic vegetation–climate interactions to better understand the impacts of such soil hydraulic changes in a model environment.

The soil moisture results below are presented for the vegetated soil fractions, as SOC stocks are dependent on vegetation inputs, and we seek to evaluate the hydroclimate responses across agricultural soils that are intended to support crop growth. Unless otherwise stated, all soil moisture changes are shown to a 0.57 m depth as a z score, relative to the mean and standard deviation of the NoLU integration at each grid cell. More specifically, the z score is taken as the difference between the 130-yr mean 2010LU or 30ST soil moisture and the 130-yr mean NoLU soil moisture, divided by the 130-yr NoLU standard deviation of soil moisture. The differences in other hydrological variables (e.g., runoff, precipitation) are similarly computed.

Significance testing was conducted using a Kolmogorov–Smirnov (KS) test at the 0.05 level, unless otherwise stated. We focus on the relative changes in the mean state between the scenarios. To focus on the responses of human-managed land systems, all maps are masked to exclude grid cells that do not have crop or pasture areas based on a modern (~2000s) land-use map.

Unauthenticated | Downloaded 03/28/23 09:33 AM UTC

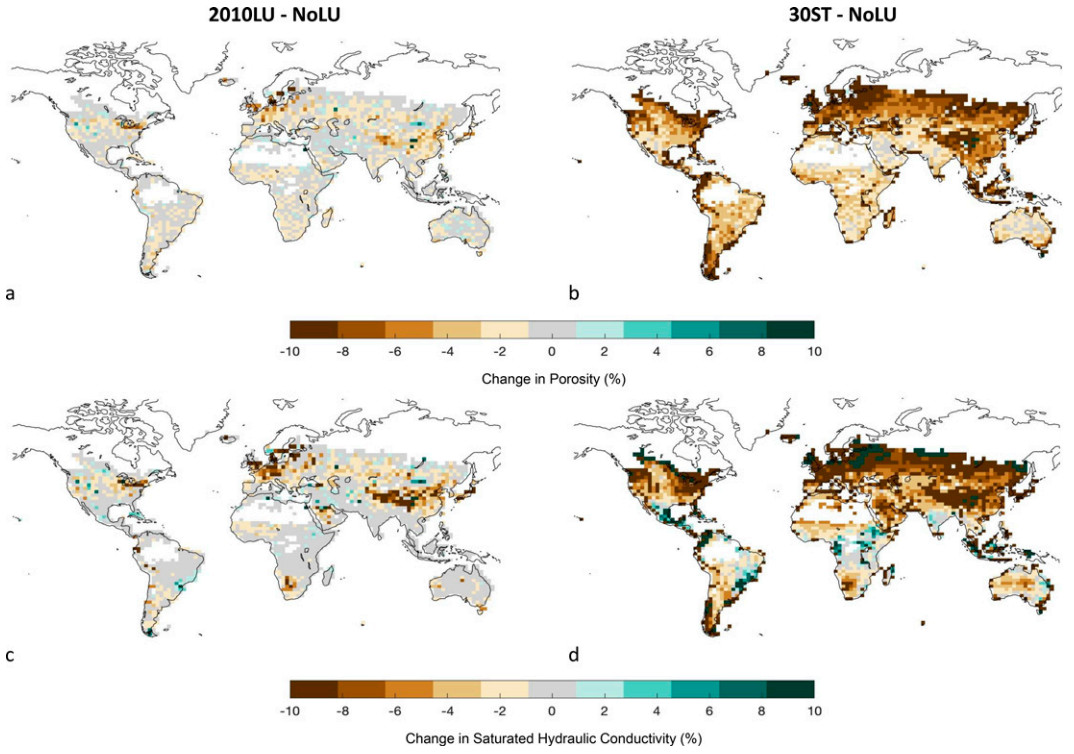


FIG. 3. Change in porosity (% change) relative to NoLU for (a) 2010LU and (b) 30ST experiments. Change in saturated hydraulic conductivity (%) from NoLU for (c) 2010LU and (d) 30ST experiments. All maps are masked for modern (2000s) crop and pasture areas.

3. Results

a. Global climatological soil moisture responses to reduced soil organic carbon contents

In the 2010LU scenarios (Figs. 4a,b), losses of organic carbon cause significant soil moisture losses of ~0.5 standard deviations or more in eastern China, parts of the Arabian Peninsula, western Europe, eastern North America, southern Africa, and northeastern Australia, with more localized negative anomalies elsewhere (southern South America). Soil moisture increases in some parts of the midlatitudes in the Northern Hemisphere, especially in central Asia/Russia. These responses, while somewhat influenced by underlying soil organic carbon changes, may be more dependent on the resulting regional circulation and precipitation changes. As expected, soil moisture declines are much more widespread in the more extreme 30ST experiment (Figs. 4b,d), where soil organic carbon stocks are reduced by 30% everywhere. Some of the strongest soil moisture losses under 30ST conditions appear in tropical forest regions, over the larger Tibetan Plateau, and at higher latitudes in Europe and North America. Overall, there is little seasonal variation in these anomalies for both scenarios.

Figure 5 shows that greater OCC reductions generally cause larger soil moisture declines. Furthermore, the few grid cells with OCC increases under 2010LU conditions also show small enhancements in soil moisture (Fig. 5a), grid cells mostly in the Northern Hemisphere midlatitudes in central North America and central Asia. Precipitation changes do not display a clear relationship to soil carbon under 2010LU conditions. While more grid cells of soil moisture decline are associated with modest precipitation declines (Fig. 5a) these variables are not very strongly associated. In other words, for many grid cells plotted across both scenarios in Fig. 5, soil moisture increases with organic carbon even while the level of precipitation change remains constant. This suggests that the soil moisture declines shown are primarily mediated through organic carbon impacts on soil hydraulic properties in these experiments instead of feedbacks to the atmosphere that result in mean changes in precipitation per grid cell. The OCC change impact on soil moisture is even more clearly demonstrated under 30ST conditions, in which all shown grid cells have lost soil carbon and the resulting OCC changes are of higher magnitude (Fig. 5b). We note that grid cells showing the largest soil moisture and OCC declines are not necessarily associated with the largest mean precipitation declines (and indeed many of these highest-loss grid cells are associated with slight increases in seasonal precipitation) (Fig. 5b).

In areas where soil moisture is most strongly impacted by 30ST OCC changes (Figs. 4b,d), precipitation does not generally display widespread strong or even significant responses (Figs. 6a,d) in either season. One exception to this occurs in northeastern Australia, where modest and significant precipitation declines are shown in April–September and do overlap with areas of OCC and soil moisture losses. Precipitation actually increases slightly in southern Africa April–September

Unauthenticated | Downloaded 03/28/23 09:33 AM UTC

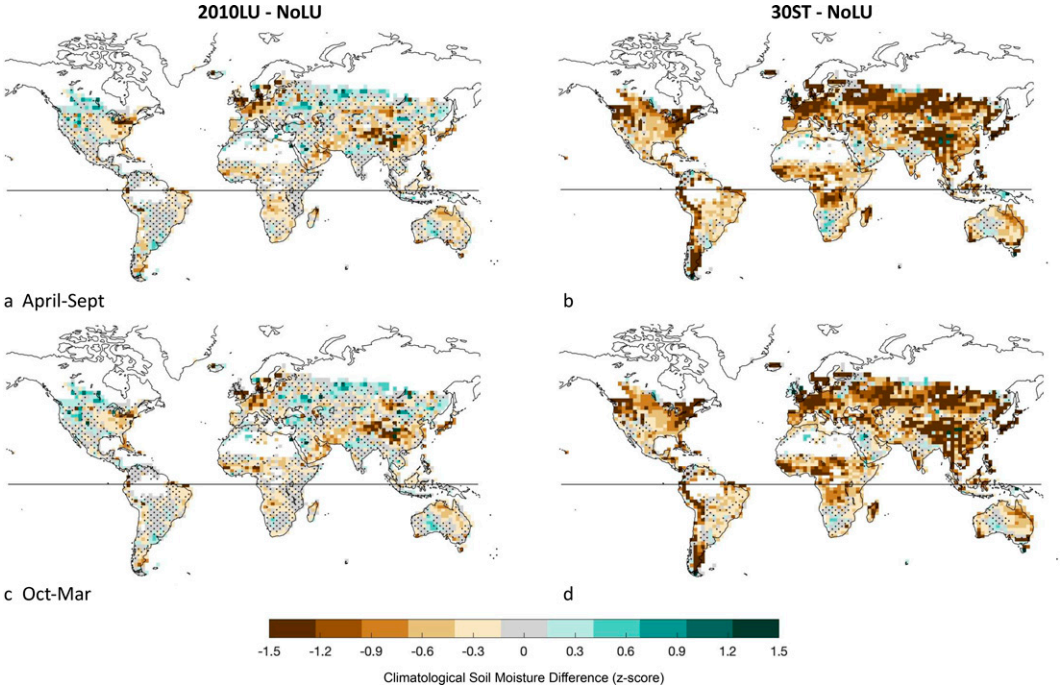


FIG. 4. Soil moisture (130-yr) climatological anomalies (z score) relative to the NoLU experiment for the (a) 2010LU experiment, April–September; (b) 30ST experiment, April–September; (c) 2010LU experiment, October–March; (d) 30ST experiment, October–March. Stippled areas are not statistically significant.

(Fig. 6a), and while soil moisture increases slightly in the same season (Fig. 4b), so does runoff and runoff efficiency (i.e., total runoff divided by precipitation) (Figs. 6b,c). Varied precipitation responses are shown across the Arabian Peninsula and northern South Asia. However, these are not highly significant likely owing to the arid and semiarid conditions where small absolute increases can result in large relative change. In the western United States and northern regions of China and East Asia, runoff displays small but significant increases in both seasons (Figs. 5b,c and 5e,f), indicating reduced infiltration that leads to declines in soil moisture (Figs. 4b,d). However, in other regions of significant soil moisture declines (Figs. 4b,d), there are few significant responses in runoff and runoff efficiency, suggesting small to negligible changes in infiltration. Soil moisture declines in the 30ST scenario in these regions are thus primarily related to reductions

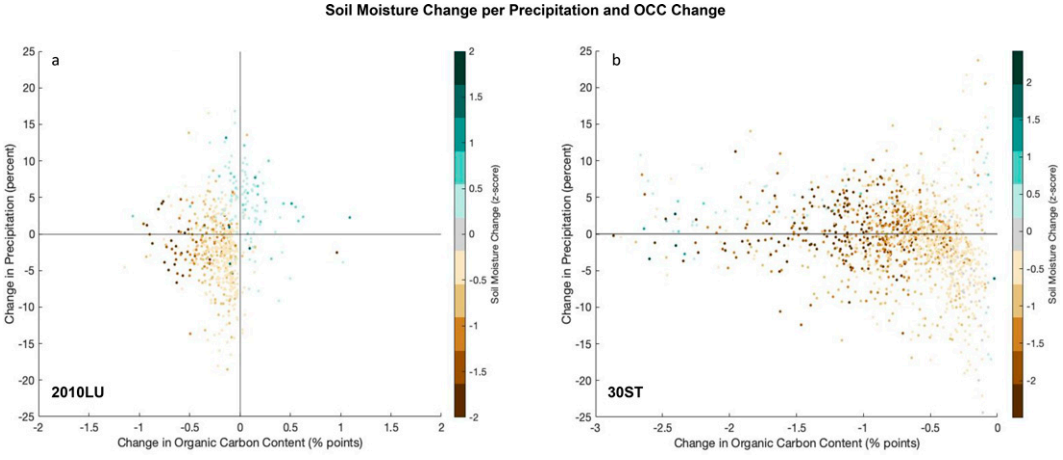


FIG. 5. Mean soil moisture change (z score on color bar) vs mean model-simulated precipitation change (%, y axis) vs organic carbon content change (percentage points, x axis) for (a) 2010LU minus NoLU and (b) 30ST minus NoLU. Only significant soil moisture anomalies (per grid cell) are plotted across both the Northern and Southern Hemispheres for their respective growing seasons.

Unauthenticated | Downloaded 03/28/23 09:33 AM UTC

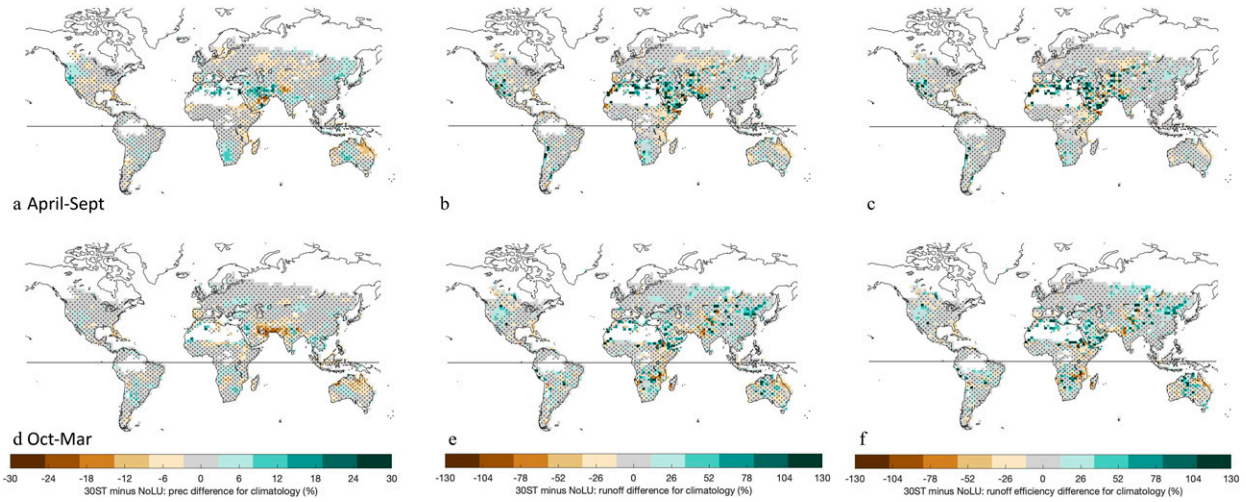


FIG. 6. Model-simulated changes due to the 30ST experiment (relative to the NoLU experiment) during April–September for (a) precipitation (%), (b) surface + below-ground runoff (%), and (c) runoff efficiency (runoff divided by precipitation) (%). (d)–(f) As in (a)–(c), but for October–March. Stippled areas are not statistically significant.

in soils' total water holding capacity (e.g., porosity) resulting from changes in organic carbon.

b. Regional climatological soil moisture responses to reduced soil organic carbon contents

Further support for the primary role of reduced water holding capacity in these experimental results is indicated in the monthly and seasonal persistence of soil moisture declines, both globally and in key areas of largest organic carbon changes (Fig. 7). Soil moisture declines resulting from changes in OCC between the experiments are also consistent across simulated years (Fig. 7a) and across the seasonal cycle in nearly all impacted regions (Figs. 7b–f). Even the relatively modest OCC declines in 2010LU (Fig. 2b) result in a

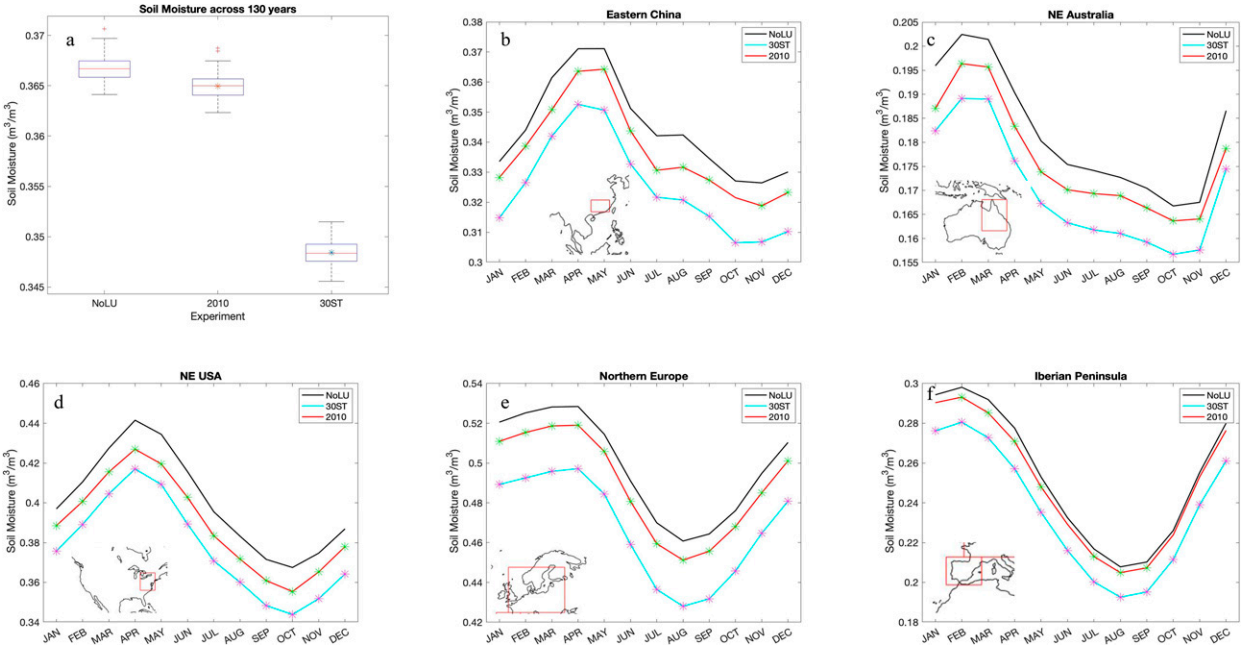


FIG. 7. (a) Boxplot distributions of annual soil moisture ($m^3\ m^{-3}$) to 57 cm depth, averaged for all land grid cells across 130 simulated years. Black asterisks denote a statistically significant difference from the NoLU case. Also shown is monthly soil moisture (mm) down to 57 cm for all three experiments for (b) eastern China, (c) northeastern Australia, (d) the northeastern United States, (e) northern Europe, and (f) the Iberian Peninsula. Black, red, and blue lines depict the NoLU, 2010LU, and 30ST experiments, respectively. Pink and green stars denote significant changes for the month indicated from NoLU for 30ST and 2010LU, respectively. Red boxes on maps in inset denote regional averages taken for line plots in (b)–(f).

Unauthenticated | Downloaded 03/28/23 09:33 AM UTC

significantly different and drier soil moisture distribution across all simulated years, although the central changes are quite small and within a few percent. As expected, the 30ST experiment further reduces soil moisture across all years (Fig. 7a), resulting in mean (and even relatively "wet") conditions that are well below even the driest soil moisture years under NoLU conditions. When isolating those regions most heavily impacted by OCC changes (Figs. 7b–f insets), we see that soil moisture declines in 2010LU and 30ST are consistent across all months in the annual cycle, and not necessarily dominated by any one month or season. These persistent reductions in monthly soil moisture occur regardless of background regional climate conditions, for example, the relatively humid conditions prevailing in northern Europe, the northeastern United States, northeastern Australia, and eastern China or the semiarid and seasonally arid conditions surrounding the Iberian Peninsula.

4. Discussion

Most agricultural soils are degraded to some extent, marked in particular by a loss of organic carbon (FAO 2021; Sanderman et al. 2017). Recent work has evaluated changes to soil carbon stocks in global climate model experiments, particularly to serve climate change mitigation (Ito et al. 2020). However, less attention has been given to the role of soil carbon in water cycling and regional hydroclimate change, which may be relevant for climate change adaptation (Iizumi and Wagai 2019). Our experiments showed that reduced soil organic carbon content across many key agricultural areas affect hydraulic parameters in ways that reduce overall soil moisture relative to NoLU conditions. In some areas, even small reductions in OCC (on the order of 0.5–1 weight % in the 2010LU case, see brown colors in Fig. 2b), can translate into declines in soil moisture of up to ~1 standard deviation of the reference NoLU soil moisture (brown colors in Figs. 4a,c). A 30% reduction in SOC stocks, within the estimated 25%–75% SOC losses characterizing most agricultural soils (Lal 2015; Lal et al. 2015; Lajtha et al. 2018), result in even larger soil moisture losses (brown colors in Figs. 4b,d) that are on par with recent (2000–20) dry climate anomalies in the American Southwest, in which soil moisture changes range from −0.77 to −2.6 standard deviations (in 2002 specifically) (Williams et al. 2020; Cook et al. 2021).

To our knowledge, these experiments are the first to explore the *hydroclimate* impacts of soil organic carbon on a global scale with a coupled (land–atmosphere) climate model that captures long-term climate variability. The soil moisture losses produced in both experiments are related to reductions in porosity, and to a lesser extent infiltration, which reduce water holding capacity. These results also imply that rebuilding soil organic carbon through improved management on agricultural lands has the potential to improve soil water holding capacity in agricultural lands, which may "buffer" against sudden droughts and dry weather anomalies (Abdallah et al. 2021; Steward et al. 2019). The future efficacy of these effects, however, will also depend on the coevolution of precipitation anomalies under climate change and interactions with natural climate variability, which in more water-limited areas could result in dry climate anomalies that extend for long periods, thereby limiting overall water supply.

However, in our experiments reduced soil water holding capacity does not necessarily lead to higher vegetation drought stress. This is partly because these reductions in soil water holding—or buffering—capacity are relatively small (albeit significant), and our simplified experimental design does not allow for much change in precipitation (see distribution across y axis in Fig. 5) and evapotranspiration (ET; due to the prescribed vegetation structure). Soil water pools temporarily store water, which is eventually "used" by soil surface evaporation, plant transpiration, and runoff. When normally saturated, a soil's water holding capacity can change the allocation between runoff and ET. However, most agricultural lands are not constantly at saturation. Thus, even though the size of the soil water buffer changes under our SOC sensitivity scenarios, the overall precipitation and total ecosystem buffer (i.e., total water stored between the soils and intercepted canopy water) is still enough to broadly maintain runoff rates within the variability NoLU runoff, with some isolated areas of significant runoff and/or runoff efficiency increases (green colors Figs. 6b,c,e,f).

Nevertheless, we emphasize that these experiments are simplified sensitivity tests. Future work is needed using dynamic vegetation, that is, where canopy development is allowed to interact more fully with environmental conditions, and to explore the impacts of SOC changes under a variety of climate anomalies (e.g., dry, hot, and wet), rather than climatological differences alone. Such experiments will likely produce different responses across the surface water balance terms, including possible areas of enhanced vegetation drought stress. For example, sudden dry climate anomalies, particularly where annual crops are planted, may result in feedbacks that further reduce soil water and/or inhibit plant growth. Stomatal closure, on the other hand, particularly under higher CO_2 concentrations (Swann 2018), may partially compensate for soil water declines that result from reduced OCC. Myriad other interactions, including irrigation and crop management, may further complicate the above vegetation–climate processes.

Future model experiments should also assess sensitivities of key hydraulic parameters, and resulting hydroclimate responses, to the choice of PTFs, which are highly parameterized and have limits to their applicability depending upon the region/locale and soil type (Montzka et al. 2017). Many PTFs exist for different soils, regions, and spatial scales. We leveraged the PTFs detailed within De Lannoy et al. (2014) primarily for their implementation over larger scales and their applicability for relatively low levels of OCC (i.e., lower than organic soils), which characterize most agricultural soils. However, we note that choosing the appropriate PTFs for the scales under consideration (e.g., in this case global climate model grids on the order of 100 km) is not straightforward and highly uncertain (Montzka et al. 2017; Minasny et al. 2017; Minasny and McBratney 2018). Recent work, for example, by Montzka et al. (2017), do nevertheless present new scaling approaches specific to individual model grids that better captures subgrid variability of soil water retention and

Unauthenticated | Downloaded 03/28/23 09:33 AM UTC

Table 1. Derivation of the Soil Bulk Density ρ_b[a]

SHP	Units	PTF
θ_{33t}	m^3/m^3	$= -0.251 \times$ sand_f $+ 0.195 \times$ clay_f $+ 0.011 \times$ OM $+ 0.006 \times$ sand_f $\times$ OM $- 0.027 \times$ clay_f $\times$ OM $+ 0.452 \times$ sand_f $\times$ clay_f $+ 0.299$
θ_{33}	m^3/m^3	$= \theta_{33t} + (1.283 \times \theta_{33t}^2 - 0.374 \times \theta_{33t} - 0.015)$
$\theta_{(s\text{-}33)t}$	m^3/m^3	$= 0.278 \times$ sand_f $+ 0.034 \times$ clay_f $+ 0.022 \times$ OM $- 0.018 \times$ sand_f $\times$ OM $- 0.027 \times$ clay_f $\times$ OM $- 0.584 \times$ sand_f $\times$ clay_f $+ 0.078$
$\theta_{(s\text{-}33)}$	m^3/m^3	$= \theta_{(s\text{-}33)t} + (0.6360 \times \theta_{(s\text{-}33)t} - 0.107)$
θ_s^*	m^3/m^3	$= \theta_{33} + \theta_{(s\text{-}33)} - 0.097 \times$ sand_f $+ 0.043$
$\boldsymbol{\rho_b}$	g/cm^3	$= (1 - \theta_s^*/0.93)\ \rho_{min}/[1 + (OM/100)\ (\rho_{min}/\rho_{OM} - 1)]$ (equation (5))

[a]The bold symbols in the left column indicate the final variables, whereas all other variables are auxiliary. The initial estimate of the soil moisture at saturation (θ_s^*) uses *Saxton and Rawls* [2006] PTFs, with sand_f, silt_f, clay_f in weight fractions and OM in weight%. This auxiliary variable θ_s^* is used to estimate ρ_b. The auxiliary variable θ_{33} is the solution for moisture at a tension of −33 kPa (θ_{33t} is a temporary first solution), $\theta_{(s\text{-}33)}$ is the solution for moisture at a tension between saturation and −33 kPa ($\theta_{(s\text{-}33)t}$ is a temporary first solution).

Table 2. Derivation of SHP Using *Wösten et al.* [1999, 2001a] PTFs With Sand, Silt, Clay, and OM in Weight% and ρ_b in g/cm^3[a]

SHP	Units	PTF
$\boldsymbol{\theta_s}$	m^3/m^3	$= 0.7919 + 0.001691 \times$ clay $- 0.29619 \times \rho_b - 0.000001491 \times$ silt$^2 + 0.0000821 \times$ OM$^2 + 0.02427 \times$ clay$^{-1} + 0.01113 \times$ silt$^{-1} + 0.01472 \times$ ln(silt) $- 0.0000733 \times$ OM $\times$ clay $- 0.000619 \times \rho_b \times$ clay $- 0.001183 \times \rho_b \times$ OM $- 0.0001664 \times$ topsoil $\times$ silt
α^*		$= -14.96 + 0.03135 \times$ clay $+ 0.0351 \times$ silt $+ 0.646 \times$ OM $+ 15.29 \times \rho_b - 0.192 \times$ topsoil $- 4.671 \times \rho_b^2 - 0.000781 \times$ clay$^2 - 0.00687 \times$ OM$^2 + 0.0449 \times$ OM$^{-1} + 0.0663 \times$ ln(silt) $+ 0.1482 \times$ ln(OM) $- 0.04546 \times \rho_b \times$ silt $- 0.4852 \times \rho_b \times$ OM $+ 0.00673 \times$ topsoil $\times$ clay
n^*		$= -25.23 - 0.02195 \times$ clay $+ 0.0074 \times$ silt $- 0.1940 \times$ OM $+ 45.5 \times \rho_b - 7.24 \times \rho_b^2 + 0.0003658 \times$ clay$^2 + 0.002885 \times$ OM$^2 - 12.81 \times \rho_b^{-1} - 0.1524 \times$ silt$^{-1} - 0.01958 \times$ OM$^{-1} - 0.2876 \times$ ln(silt) $- 0.0709 \times$ ln(OM) $- 44.6 \times$ ln(ρ_b) $- 0.02264 \times \rho_b \times$ clay $+ 0.0896 \times \rho_b \times$ OM $+ 0.00718 \times$ topsoil $\times$ clay
K_s^*		$= 7.755 + 0.0352 \times$ silt $+ 0.93 \times$ topsoil $- 0.967 \times \rho_b^2 - 0.000484 \times$ clay$^2 - 0.000322 \times$ silt$^2 + 0.001 \times$ silt$^{-1} - 0.0748 \times$ OM$^{-1} - 0.643 \times$ ln(silt) $- 0.01398 \times \rho_b \times$ clay $- 0.1673 \times \rho_b \times$ OM $+ 0.02986 \times$ topsoil $\times$ clay $- 0.03305 \times$ topsoil $\times$ silt
α	1/m	$= \exp(\alpha^*)$
n		$= \exp(n^*) + 1$
$\mathbf{K_s}$	m/s	$= 0.01 \exp(K_s^*)/(3600 \times 24)$
b		$= 1/(n - 1)$
$\boldsymbol{\psi_s}$	m H_2O	$= -0.01/\alpha$

[a]Use topsoil = 1 to obtain SHPs for the (0–30 cm) surface layer and topsoil = 0 to obtain SHPs for the (30–100 cm) subsurface layer. The bold symbols in the left column indicate final *Campbell* [1974] SHP values, whereas all other variables are temporary in the calculation of the SHP. The *van Genuchten* [1980] parameters are θ_s, α, n, and K_s; the *Campbell* [1974] parameters are θ_s, ψ_s, b, and K_s.

FIG. A1. Tables of relations used in our calculations of soil SHPs, taken/reprinted from De Lannoy et al. (2014), which were in turn based on van Genuchten (1980) and Campbell (1974).

conductivity curves. Such methods should be employed in future GCM experiments like ours, alongside systematic sensitivity testing of different PTFs. Ideally, this would be done with a higher-resolution climate model, as the coarseness of our 2° × 2.5° experiments limits capturing detailed soil attribute information and thus important regional heterogeneity in soil water responses.

There also exist large uncertainties and gaps in the soil data required for such experiments that, if not easily reduced, must be assessed and quantified. For example, feedbacks exist between SOC and soil bulk density, which were not explicitly captured in the methods we use here. Namely, a loss of SOC can increase the bulk density, which further limits soil water holding capacity (e.g., by reducing porosity). In comparing the bulk density we calculated for 2010LU conditions to the bulk density computed by De Lannoy et al. (2014) (using the PTFs they provide, Fig. A1; our difference shown in Fig. A2), we find that we underestimate the bulk density across most global areas, leading potentially to a slightly more conservative estimate of the impact on soil water. Improved methods to obtain corresponding bulk densities with OCC scenarios are, nevertheless, needed. Beyond the bulk densities, there are also large differences in SOC and soil texture data between different global soil data products, particularly at higher latitudes and over relatively carbon-rich soils (which were not the primary focus on this study, but for which new data are becoming increasingly available) (Tifafi et al. 2018; Xu et al. 2017).

Our study leveraged the SOC scenarios of Sanderman et al. (2017) that consider the effects of anthropogenic land use. However, our model implementation is not dependent on these data, and comparing land water balance results and uncertainty across other and soil data and scenarios, both global and regional, is warranted. As a longer-term model development goal, simulated soil water may also be made to depend on prognostically produced soil carbon fields from coupled, dynamic land biogeochemistry models, which are rapidly increasing in capacity and being applied to studies of future climate change mitigation.

Last, we note that soil water retention is not just a function of SOC (i.e., organic matter in various stages of decomposition), but also of other biological material in soils (e.g., cover crops with live roots and soil macrofauna) and management decisions impacting them (Michler et al. 2019; Steward et al. 2019). For example, Franzluebbers (2002) demonstrated that an increase in infiltration in long-term no-till fields (compared to conventional tillage) was primarily driven by the decrease in bulk density associated with the lack of soil disturbance (i.e., recovery from compaction), not the increase in SOC in the soil surface horizon. Our results suggest that restoring SOC alone, particularly where losses approximate our 30ST experiment, can increase infiltration rate through changes in bulk density and aggregation and can therefore serve as a targeted management goal. Additionally, there exist a variety of management practices that both build SOC and significantly

Unauthenticated | Downloaded 03/28/23 09:33 AM UTC

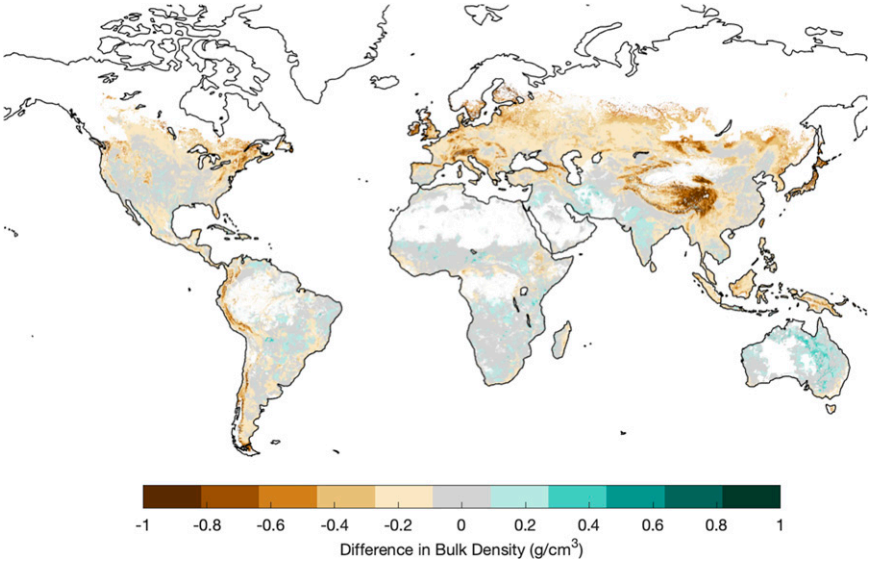


FIG. A2. Difference in bulk density for the top 30 cm of soil column taken as SoilGrids minus De Lannoy et al. (2014). Both bulk densities were computed using the PTFs described in De Lannoy et al.'s (2014) Table 1 (see Fig. A1 above) and featured in step 2 of our methods in section 2b but used different input textural and organic carbon datasets. Data are presented at 5 arc min resolution, which is the resolution of the SoilGrids provided textures and Sanderman et al. (2017) SOC scenarios.

impact soil water properties, and these may warrant representation in large-scale, process-based modeling of regional hydroclimates, particularly agricultural regions, and their responses to drought.

5. Conclusions

We used the NASA GISS ModelE global climate model to conduct a set of novel sensitivity tests evaluating hydroclimate responses to soil degradation, represented by scenarios of soil organic carbon changes across managed soils. We found that reductions in soil organic carbon reduced porosity across managed lands, leading to significant soil moisture reductions at regional scales. These losses in soil moisture were amplified under higher levels of SOC loss. Our experiments did not test the impact of dynamic vegetation in response to the reduced soil water holding capacity, but such work is critical to evaluate the full impact and importance of soil carbon in agroecosystem water cycling at global and regional scales and under climate change. Ultimately, improving the linkages between climate-model-simulated biogeophysical responses (e.g., in hydroclimate) to biogeochemical processes (e.g., vegetation and soil organic carbon) is an important forefront of land surface modeling, particularly where and when agricultural land management is a focus. This model development need becomes even more salient when considering the proliferation of recent calls motivating SOC restoration on agricultural soils for climate mitigation and *adaptation* goals (Amelung et al. 2020). The latter is related not just to improved nutrient cycling but also water provisioning, particularly in times of drought, which stand to increase even under modest climate change trajectories (Cook et al. 2021, 2020). This study demonstrates a novel application of SOC–soil water linkages for climate model simulations, with significant effects, that warrants both further development and inclusion in land-use and land-cover change modeling experiments.

Acknowledgments. SM, EW, MP, and BIC are supported by NASA Modeling, Analysis, and Prediction program (80NSSC21K1497). Resources supporting this work were provided by the NASA High-End Computing (HEC) Program through the NASA Center for Climate Simulation (NCCS) at Goddard Space Flight Center. The authors also thank Dr. Nancy Kiang for discussions and input on this work. The authors declare no conflicts of interest.

Data availability statement. ModelE soil texture, organic carbon, and saturated hydraulic parameters, alongside all experimental outputs used in this study, are openly available at https://doi.org/10.5281/zenodo.5847185.

APPENDIX

Additional Methodological Details and Description of the Land Module within ModelE

Underground runoff is computed per soil layer using the formulations of Abramopoulos et al. (1988), and depends on the 1) hydraulic conductivity, 2) average slope of a grid cell, and 3) average distance between sinks that can remove subsurface flow from the grid cell. We defined a threshold of rainfall rate ($0.22d - 5$ m s^{-1}) for different patterns of

Unauthenticated | Downloaded 03/28/23 09:33 AM UTC

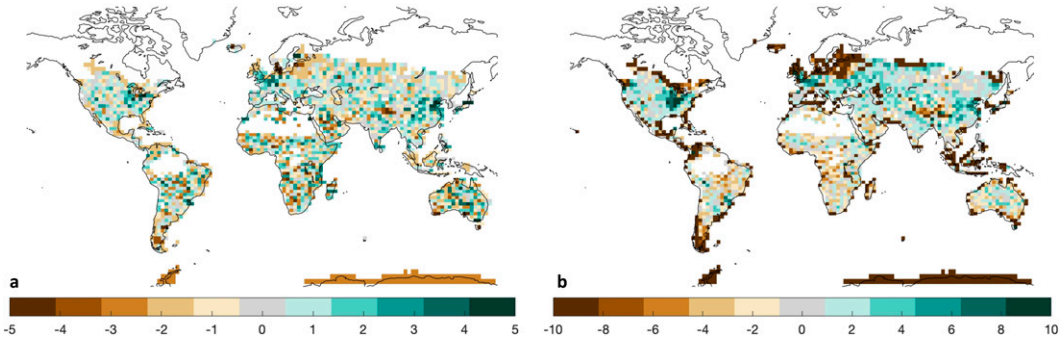


FIG. A3. Percent changes in matric potential (m H_2O) under (a) 2010LU conditions (relative to NoLU) and (b) for 30ST minus NoLU.

surface runoff generation. When rainfall rate is below this threshold, runoff happens only when the first soil layer is saturated and the percolation rate is lower than rainfall rate. When rainfall rate is above threshold, surface runoff occurs even if the first soil layer is not saturated.

Latent heat fluxes from the surface are separated between the vegetated and nonvegetated portions of each grid cell. For vegetated grid cell fractions, the evapotranspiration term is the sum of four components: transpiration, canopy evaporation from leaf surfaces, soil evaporation, and snow sublimation. Transpiration follows an aerodynamic formulation specified in Hansen et al. (1983) and Rosenzweig and Abramopoulos (1997), which is dependent on canopy conductance, atmospheric conductance, and the saturated and unsaturated air humidity. For soil evaporation under the canopy, a modification is made to the turbulent transfer coefficient to account for wind–leaf interactions. For the bare soil fraction of the grid cell, evaporation occurs as the minimum of the Penman potential evaporation or Gardner–Hillel diffusivity (Abramopoulos et al. 1988). Canopy evaporation is assumed to occur at the potential rate.

For our soil parameterization, we include here changes in additional key saturated hydraulic parameters resulting from our SOC scenarios, namely: matric potential, conductivity, and the b parameter. These were calculated based on the SOC maps described in the methods section (section 2) in the main manuscript (converted first to OCC and then to organic matter content using a scaling factor of 1.72) and the pedotransfer functions per De Lannoy et al. (2014) [see Fig. A1, shown here as adaptations of Tables 1 and 2 in De Lannoy et al. (2014)]. These saturated hydraulic parameters were then used in the model to compute the time-varying hydraulic parameters following the Campbell (1974) constitutive relationships relating soil moisture content (θ) to matric potential (ψ) and hydraulic conductivity (K), that is,

$$\psi/\psi_s = (\theta/\theta_s)^{-b} \quad \text{and}$$

$$K = K_s(\theta/\theta_s)^{2b+3}.$$

Figure A1, adapted from De Lannoy et al (2014), details the pedotransfer functions implemented in ModelE in order to obtain the saturated values of key hydraulic parameters: porosity, saturated hydraulic conductivity, and matric potential in addition to the intermediate values for soil bulk density used in the calculations (see methods in section 2 in the main manuscript).

Figure A2 shows that our computed bulk densities (as detailed in the methods in section 2 in the main manuscript) are largely lower than that of De Lannoy et al. (2014). We therefore interpret this to mean that we are taking a conservative approach, with likely underestimates of the impact of SOC losses across the growing regions that we highlight (see discussion in section 4 in the main manuscript).

Figure A3 shows increases in matric potential between our scenarios of reduced SOC and the NoLU scenario. This is consistent with the changes in saturated hydraulic variables shown in Fig. 2 in the main manuscript, and overall indicate potential losses in soil water and more challenging conditions for plant water uptake.

REFERENCES

Abdallah, A. M., H. S. Jat, M. Choudhary, E. F. Abdelaty, P. C. Sharma, and M. L. Jat, 2021: Conservation agriculture effects on soil water holding capacity and water-saving varied with management practices and agroecological conditions: A review. *Agronomy*, 11, 1681, https://doi.org/10.3390/agronomy11091681.

Abramopoulos, F., C. Rosenzweig, and B. Choudhury, 1988: Improved ground hydrology calculations for Global Climate Models (GCMs): Soil water movement and evapotranspiration. *J. Climate*, **1**, 921–941, https://doi.org/10.1175/1520-0442(1988)001<0921:IGHCFG>2.0.CO;2.

Amelung, W., and Coauthors, 2020: Towards a global-scale soil climate mitigation strategy. *Nat. Commun.*, **11**, 5427, https://doi.org/10.1038/s41467-020-18887-7.

Arenas-Calle, L. N., J. Ramirez-Villegas, S. Whitfield, and A. J. Challinor, 2021: Design of a Soil-based Climate-Smartness Index (SCSI) using the trend and variability of yields and soil organic carbon. *Agric. Syst.*, **190**, 103086, https://doi.org/10.1016/j.agsy.2021.103086.

Ball, J. T., I. E. Woodrow, and J. A. Berry, 1987: A model predicting stomatal conductance and its contribution to the control of photosynthesis under different environmental conditions. *Progress in Photosynthesis Research*, J. Biggins, Ed., Springer, 221–224, https://doi.org/10.1007/978-94-017-0519-6_48.

Unauthenticated | Downloaded 03/28/23 09:33 AM UTC

Basche, A. D., and M. S. DeLonge, 2019: Comparing infiltration rates in soils managed with conventional and alternative farming methods: A meta-analysis. *PLOS ONE*, **14**, e0215702, https://doi.org/10.1371/journal.pone.0215702.

Blanco-Canqui, H., T. M. Shaver, J. L. Lindquist, C. A. Shapiro, R. W. Elmore, C. A. Francis, and G. W. Hergert, 2015: Cover crops and ecosystem services: Insights from studies in temperate soils. *Agron. J.*, **107**, 2449–2474, https://doi.org/10.2134/agronj15.0086.

Bossio, D. A., and Coauthors, 2020: The role of soil carbon in natural climate solutions. *Nat. Sustainability*, **3**, 391–398, https://doi.org/10.1038/s41893-020-0491-z.

Campbell, G. S., 1974: A simple method for determining unsaturated conductivity from moisture retention data. *Soil Sci.*, **117**, 311–314, https://doi.org/10.1097/00010694-197406000-00001.

Cardoso, E. J. B. N., and Coauthors, 2013: Soil health: Looking for suitable indicators. What should be considered to assess the effects of use and management on soil health? *Sci. Agric.*, **70**, 274–289, https://doi.org/10.1590/S0103-90162013000400009.

Chabbi, A., and Coauthors, 2017: Aligning agriculture and climate policy. *Nat. Climate Change*, **7**, 307–309, https://doi.org/10.1038/nclimate3286.

Collatz, G. J., J. T. Ball, C. Grivet, and J. A. Berry, 1991: Physiological and environmental regulation of stomatal conductance, photosynthesis and transpiration: A model that includes a laminar boundary layer. *Agric. For. Meter.*, **54**, 107–136, https://doi.org/10.1016/0168-1923(91)90002-8.

Cook, B. I., J. S. Mankin, K. Marvel, A. P. Williams, J. E. Smerdon, and K. J. Anchukaitis, 2020: Twenty-first century drought projections in the CMIP6 forcing scenarios. *Earth's Future*, **8**, e2019EF001461, https://doi.org/10.1029/2019EF001461.

——, ——, A. P. Williams, K. D. Marvel, J. E. Smerdon, and H. Liu, 2021: Uncertainties, limits, and benefits of climate change mitigation for soil moisture drought in southwestern North America. *Earth's Future*, **9**, e2021EF002014, https://doi.org/10.1029/2021EF002014.

De Lannoy, G. J. M., R. D. Koster, R. H. Reichle, S. P. P. Mahanama, and Q. Liu, 2014: An updated treatment of soil texture and associated hydraulic properties in a global land modeling system. *J. Adv. Model. Earth Syst.*, **6**, 957–979, https://doi.org/10.1002/2014MS000330.

Drewniak, B. A., U. Mishra, J. Song, J. Prell, and V. R. Kotamarthi, 2015: Modeling the impact of agricultural land use and management on US carbon budgets. *Biogeosciences*, **12**, 2119–2129, https://doi.org/10.5194/bg-12-2119-2015.

Eyring, V., S. Bony, G. A. Meehl, C. Senior, B. Stevens, R. J. Stouffer, and K. E. Taylor, 2016: Overview of the Coupled Model Intercomparison Project Phase 6 (CMIP6) experimental design and organisation. *Geosci. Model Dev.*, **9**, 1937–1958, https://doi.org/10.5194/gmd-9-1937-2016.

FAO, 2021: The state of the world's land and water resources for food and agriculture 2021—Systems at breaking point. FAO, 393 pp., https://doi.org/10.4060/cb9910en.

Farquhar, G. D., and S. von Caemmerer, 1982: Modelling of photosynthetic response to environmental conditions. *Physiological Plant Ecology II*, O. L. Lange et al., Eds., Encyclopedia of Plant Physiology 920, Vol. 12/B, Springer, 549–587, https://doi.org/10.1007/978-3-642-68150-9_17.

Franzluebbers, A. J., 2002: Soil organic matter stratification ratio as an indicator of soil quality. *Soil Tillage Res.*, **66**, 95–106, https://doi.org/10.1016/S0167-1987(02)00018-1.

Friend, A. D., and N. Y. Kiang, 2005: Land surface model development for the GISS GCM: Effects of improved canopy physiology on simulated climate. *J. Climate*, **18**, 2883–2902, https://doi.org/10.1175/JCLI3425.1.

Hansen, J., G. Russell, D. Rind, P. Stone, A. Lacis, S. Lebedeff, R. Ruedy, and L. Travis, 1983: Efficient three-dimensional global models for climate studies: Models I and II. *Mon. Wea. Rev.*, **111**, 609–662, https://doi.org/10.1175/1520-0493(1983)111<0609:ETDGMF>2.0.CO;2.

Hengl, T., and Coauthors, 2017: SoilGrids250m: Global gridded soil information based on machine learning. *PLOS ONE*, **12**, e0169748, https://doi.org/10.1371/journal.pone.0169748.

Herrick, J. E., O. E. Sala, and J. W. Karl, 2013: Land degradation and climate change: A sin of omission? *Front. Ecol. Environ.*, **11**, 283–283, https://doi.org/10.1890/1540-9295-11.6.283.

Hillel, D., and C. Rosenzweig, 2011: The role of soils in climate change. *Handbook of Climate Change and Agroecosystems: Impacts, Adaptation and Mitigation*, D. Hillel and C. Rosenzweig, Eds., Imperial College Press, 9–20.

Houghton, R. A., and A. A. Nassikas, 2017: Global and regional fluxes of carbon from land use and land cover change 1850–2015. *Global Biogeochem. Cycles*, **31**, 456–472, https://doi.org/10.1002/2016GB005546.

Hudson, B. D., 1994: Soil organic matter and available water capacity. *J. Soil Water Conserv.*, **49**, 189–194.

Iizumi, T., and R. Wagai, 2019: Leveraging drought risk reduction for sustainable food, soil and climate via soil organic carbon sequestration. *Sci. Rep.*, **9**, 19744, https://doi.org/10.1038/s41598-019-55835-y.

Intergovernmental Technical Panel on Soils, 2015: Status of the world's soil resources: Main report. FAO, 650 pp., http://www.fao.org/3/a-i5199e.pdf.

Ito, A., and Coauthors, 2020: Soil carbon sequestration simulated in CMIP6-LUMIP models: Implications for climatic mitigation. *Environ. Res. Lett.*, **15**, 124061, https://doi.org/10.1088/1748-9326/abc912.

Kane, D. A., M. A. Bradford, E. Fuller, E. E. Oldfield, and S. A. Wood, 2021: Soil organic matter protects US maize yields and lowers crop insurance payouts under drought. *Environ. Res. Lett.*, **16**, 044018, https://doi.org/10.1088/1748-9326/abe492.

Kelley, M., and Coauthors, 2020: GISS-E2.1: Configurations and climatology. *J. Adv. Model. Earth Syst.*, **12**, e2019MS002025, https://doi.org/10.1029/2019MS002025.

Kim, Y., P. R. P. Moorcroft, I. Aleinov, M. J. Puma, and N. Y. Kiang, 2015: Variability of phenology and fluxes of water and carbon with observed and simulated soil moisture in the Ent Terrestrial Biosphere Model (Ent TBM version 1.0.1.0.0). *Geosci. Model Dev.*, **8**, 3837–3865, https://doi.org/10.5194/gmd-8-3837-2015.

Krull, E. S., J. O. Skjemstad, and J. A. Baldock, 2004: Functions of soil organic matter and the effect on soil properties. CSIRO, 124 pp., https://publications.csiro.au/rpr/download?pid=procite:558be5ab-e649-4163-b537-153958000418&dsid=DS1.

Lajtha, K., and Coauthors, 2018: Soils. *Second State of the Carbon Cycle Report (SOCCR2): A Sustained Assessment Report*, N. Cavallaro et al., Eds., U.S. Global Change Research Program, 469–506, https://doi.org/10.7930/SOCCR2.2018.Ch12.

Lal, R., 2015: Restoring soil quality to mitigate soil degradation. *Sustainability*, **7**, 5875–5895, https://doi.org/10.3390/su7055875.

——, R. F. Follett, B. A. Stewart, and J. M. Kimble, 2007: Soil carbon sequestration to mitigate climate change and advance

Unauthenticated | Downloaded 03/28/23 09:33 AM UTC

food security. *Soil Sci.*, **172**, 943–956, https://doi.org/10.1097/ss.0b013e31815cc498.

——, J. Delgado, P. M. Groffman, N. Millar, and C. Dell, 2011: Management to mitigate and adapt to climate change. *J. Soil Water Conserv.*, **66**, 276–285, https://doi.org/10.2489/jswc.66.4.276.

——, W. Negassa, and K. Lorenz, 2015: Carbon sequestration in soil. *Curr. Opin. Environ. Sustainability*, **15**, 79–86, https://doi.org/10.1016/j.cosust.2015.09.002.

Loveland, P., and J. Webb, 2003: Is there a critical level of organic matter in the agricultural soils of temperate regions: A review. *Soil Tillage Res.*, **70**, 1–18, https://doi.org/10.1016/S0167-1987(02)00139-3.

Luo, Y., and Coauthors, 2016: Toward more realistic projections of soil carbon dynamics by Earth system models. *Global Biogeochem. Cycles*, **30**, 40–56, https://doi.org/10.1002/2015GB005239.

Manns, H. R., G. W. Parkin, and R. C. Martin, 2016: Evidence of a union between organic carbon and water content in soil. *Can. J. Soil Sci.*, **96**, 305–316, https://doi.org/10.1139/cjss-2015-0084.

McDermid, S. S., C. Montes, B. I. Cook, M. J. Puma, N. Y. Kiang, and I. Aleinov, 2019: The sensitivity of land–atmosphere coupling to modern agriculture in the northern midlatitudes. *J. Climate*, **32**, 465–484, https://doi.org/10.1175/JCLI-D-17-0799.1.

Michler, J. D., K. Baylis, M. Arends-Kuenning, and K. Mazvimavi, 2019: Conservation agriculture and climate resilience. *J. Environ. Econ. Manage.*, **93**, 148–169, https://doi.org/10.1016/j.jeem.2018.11.008.

Miller, R. L., 2014: CMIP5 historical simulations (1850–2012) with GISSModelE2 Ron. *J. Adv. Model. Earth Syst.*, **6**, 441–477, https://doi.org/10.1002/2013MS000266.

Minasny, B., and A. B. McBratney, 2018: Limited effect of organic matter on soil available water capacity. *Eur. J. Soil Sci.*, **69**, 39–47, https://doi.org/10.1111/ejss.12475.

——, and Coauthors, 2017: Soil carbon 4 per mille. *Geoderma*, **292**, 59–86, https://doi.org/10.1016/j.geoderma.2017.01.002.

Montzka, C., M. Herbst, L. Weihermüller, A. Verhoef, and H. Vereecken, 2017: A global data set of soil hydraulic properties and sub-grid variability of soil water retention and hydraulic conductivity curves. *Earth Syst. Sci. Data*, **9**, 529–543, https://doi.org/10.5194/essd-9-529-2017.

Oldfield, E. E., M. A. Bradford, and S. A. Wood, 2019: Global meta-analysis of the relationship between soil organic matter and crop yields. *SOIL*, **5**, 15–32, https://doi.org/10.5194/SOIL-5-15-2019.

Paustian, K., J. Lehmann, S. Ogle, D. Reay, G. P. Robertson, and P. Smith, 2016: Climate-smart soils. *Nature*, **532**, 49–57, https://doi.org/10.1038/nature17174.

Puma, M. J., I. Rodriguez-Iturbe, M. A. Celia, A. J. Guswa, M. J. Puma, I. R. Iturbe, M. A. Celia, and A. J. Guswa, 2007: Implications of rainfall temporal resolution for soil-moisture and transpiration modeling. *Transp. Porous Media*, **68**, 37–67, https://doi.org/10.1007/s11242-006-9057-4.

Rawls, W. J., Y. Pachepsky, J. C. Ritchie, T. M. Sobecki, and H. Bloodworth, 2003: Effect of soil organic carbon on soil water retention. *Geoderma*, **116**, 61–76, https://doi.org/10.1016/S0016-7061(03)00094-6.

Rosenzweig, C., and F. Abramopoulos, 1997: Land-surface model development for the GISS GCM. *J. Climate*, **10**, 2040–2054, https://doi.org/10.1175/1520-0442(1997)010<2040:LSMDFT>2.0.CO;2.

Sanderman, J., T. Hengl, and G. J. Fiske, 2017: Soil carbon debt of 12,000 years of human land use. *Proc. Natl. Acad. Sci. USA*, **114**, 9575–9580, https://doi.org/10.1073/pnas.1706103114.

Saxton, K. E., and W. J. Rawls, 2006: Soil water characteristic estimates by texture and organic matter for hydrologic solutions. *Soil. Sci. Soc. Amer. J.*, **70**, 1569–1578, https://doi.org/10.2136/sssaj2005.0117.

Schmidt, G. A., and Coauthors, 2014: Configuration and assessment of the GISS ModelE2 contributions to the CMIP5 archive. *J. Adv. Model. Earth Syst.*, **6**, 141–184, https://doi.org/10.1002/2013MS000265.

Scholes, R., and Coauthors, 2018: Summary for policymakers. The Assessment Report on Land Degradation and Restoration of the Intergovernmental Science-Policy Platform on Biodiversity and Ecosystem Services, IPBES Secretariat, 44 pp., https://www.fs.usda.gov/research/publications/misc/94550_2018_scholes.pdf.

Staub, B., C. Rosenzweig, and D. Rind, 1987: Global digital data sets of soil type, soil texture, surface slope, and other properties: Documentation of archived data tape. NASA Tech Memo. 100685, 20 pp., https://ntrs.nasa.gov/api/citations/19880007713/downloads/19880007713.pdf.

Steward, P. R., C. Thierfelder, A. J. Dougill, and I. Ligowe, 2019: Conservation agriculture enhances resistance of maize to climate stress in a Malawian medium-term trial. *Agric. Ecosyst. Environ.*, **277**, 95–104, https://doi.org/10.1016/j.agee.2018.07.009.

Swann, A. L. S., 2018: Plants and drought in a changing climate. *Curr. Climate Change Rep.*, **4**, 192–201, https://doi.org/10.1007/s40641-018-0097-y.

Tian, H., and Coauthors, 2016: The terrestrial biosphere as a net source of greenhouse gases to the atmosphere. *Nature*, **531**, 225–228, https://doi.org/10.1038/nature16946.

Tifafi, M., B. Guenet, and C. Hatté, 2018: Large differences in global and regional total soil carbon stock estimates based on SoilGrids, HWSD, and NCSCD: Intercomparison and evaluation based on field data from USA, England, Wales, and France. *Global Biogeochem. Cycles*, **32**, 42–56, https://doi.org/10.1002/2017GB005678.

van Genuchten, M., 1980: A closed-form equation for predicting the hydraulic conductivity of unsaturated soils. *Soil Sci. Soc. Amer. J.*, **44**, 892, https://doi.org/10.2136/sssaj1980.03615995004400050002x.

Webb, N. P., N. A. Marshall, L. C. Stringer, M. S. Reed, A. Chappell, and J. E. Herrick, 2017: Land degradation and climate change: Building climate resilience in agriculture. *Front. Ecol. Environ.*, **15**, 450–459, https://doi.org/10.1002/fee.1530.

Webb, R. S., C. E. Rosenzmig, and E. R. Levine, 1991: A global data set of soil particle size properties. NASA Tech Memo. 4286, 33 pp., https://ntrs.nasa.gov/api/citations/19910021275/downloads/19910021275.pdf.

——, C. E. Rosenzweig, and E. R. Levine, 1993: Specifying land surface characteristics in general circulation models: Soil profile data set and derived water-holding capacities. *Global Biogeochem. Cycles*, **7**, 97–108, https://doi.org/10.1029/92GB01822.

Williams, A., and Coauthors, 2016: Soil water holding capacity mitigates downside risk and volatility in US rainfed maize: Time to invest in soil organic matter? *PLOS ONE*, **11**, e0160974, https://doi.org/10.1371/journal.pone.0160974.

Williams, A. P., and Coauthors, 2020: Large contribution from anthropogenic warming to an emerging North American megadrought. *Science*, **368**, 314–318, https://doi.org/10.1126/science.aaz9600.

Unauthenticated | Downloaded 03/28/23 09:33 AM UTC

Wösten, J. H. M., A. Lilly, A. Nemes, and C. Le Bas, 1999: Development and use of a database of hydraulic properties of European soils. *Geoderma*, **90**, 169–185, https://doi.org/10.1016/S0016-7061(98)00132-3.

——, Y. A. Pachepsky, and W. J. Rawls, 2001: Pedotransfer functions: Bridging the gap between available basic soil data and missing soil hydraulic characteristics. *J. Hydrol.*, **251**, 123–150, https://doi.org/10.1016/S0022-1694(01)00464-4.

Xu, J., P. J. Morris, J. Liu, and J. Holden, 2017: PEATMAP: Refining estimates of global peatland distribution based on a meta-analysis. *Catena*, 160, 134–140, https://doi.org/10.1016/j.catena.2017.09.010.

Yost, J. L., and A. E. Hartemink, 2019: Effects of carbon on moisture storage in soils of the Wisconsin Central Sands, USA. *Eur. J. Soil Sci.*, **70**, 565–577, https://doi.org/10.1111/ejss.12776.

Zomer, R. J., D. A. Bossio, R. Sommer, and L. V. Verchot, 2017: Global sequestration potential of increased organic carbon in cropland soils. *Sci. Rep.*, **7**, 15554, https://doi.org/10.1038/s41598-017-15794-8.

Unauthenticated | Downloaded 03/28/23 09:33 AM UTC